Irradiance Monitoring for Bifacial PV Systems' Performance and Capacity Testing

Chris Deline, Silvana Ovaitt, Michael Gostein, Jennifer Braid, Jeff Newmiller, and Itai Suez

***Abstract*—Three standards for photovoltaic (PV) performance and capacity testing are evaluated for bifacial PV system reporting: performance ratio, ASTM E2848, and a new draft of IEC 61724-2. In this context, challenges and recommendations for rear irradiance instrumentation are described for three types of bifacial irradiance sensors—horizontal albedometer, backward-facing reference cells (or pyranometer), and bifacial reference module. A year of operating field data for single-axis tracked bifacial and monofacial systems was collected, including periods of high surface albedo due to snow ground cover. If snowy conditions are included, we found that all three methods performed comparably to the monofacial baseline case, but only if rear-measured irradiance is incorporated into the expected energy calculation. The lowest RMS error was obtained by following the draft IEC 61724-2 standard and using a calibrated bifacial reference module for bifacial irradiance resource. If measured rear irradiance is unavailable, field conditions either need to be filtered to avoid variable (snowy) albedo or an albedometer measurement can be used in conjunction with modeled rear irradiance along with the draft IEC procedure. Additional practical factors are described, including the proper placement of rear irradiance sensors and the proper interpretation of IEC 61724-1 bifacial performance ratio calculations.**

***Index Terms*—Bifacial PV, capacity testing, IEC 61724, photovoltaic systems.**

I. Introduction

THE photovoltaic (PV) industry is rapidly adopting bifacial PV modules, which since 2023 already make up a majority of global module production [1] and whose dominance will continue in the near term [2], [3]. However, best practices for irradiance monitoring and performance testing of bifacial systems have not yet reached widespread consensus due to technical challenges [4], [5].

Manuscript received 5 April 2024; revised 21 June 2024; accepted 8 July 2024. Date of publication 30 July 2024; date of current version 26 August 2024. This work was supported in part by the U.S. Department of Energy's Solar Energy Technologies Office under Award Number DE-SC0020831, in part by the National Renewable Energy Laboratory, operated by Alliance for Sustainable Energy, LLC, for the U.S. Department of Energy (DOE) under Grant DE-AC36-08GO28308, and in part by the U.S. Department of Energy's Office of Energy Efficiency and Renewable Energy (EERE) under Solar Energy Technologies Office (SETO) Agreement Number 38535. *(Corresponding author: Chris Deline.)*

Chris Deline and Silvana Ovaitt are with National Renewable Energy Laboratory, Golden, CO 80401 USA (e-mail: chris.deline@nrel.gov).

Michael Gostein is with Atonometrics, Austin, TX 78757 USA.

Jennifer Braid is with Sandia National Laboratories, Albuquerque, NM 87123 USA.

Jeff Newmiller is with the DNV, Oakland, CA 94612 USA.

Itai Suez is with Create Energy, Portland, TN 37148 USA.

Color versions of one or more figures in this article are available at https://doi.org/10.1109/JPHOTOV.2024.3430551.

Digital Object Identifier 10.1109/JPHOTOV.2024.3430551

Bifacial modules can have significant performance advantages over conventional monofacial modules because their transparent rear surfaces used in concert with bifacial solar cell designs enable them to absorb light from both sides. Ground-reflected and sky-diffuse irradiance incidents on the rear side of bifacial modules increase their total light collected, with bifacial energy gain relative to monofacial modules typically ranging from 5% to 12% for single-axis-tracked systems [6], [7].

Performance or capacity testing is critical to validating the economics and bankability of utility-scale PV projects and is a key requirement in contractual arrangements between developers, owners, operators, and engineering, procurement, and construction companies. Performance testing involves computing system metrics that quantify measured energy against expected energy, which, in turn, must be estimated using monitored irradiance as an input to system performance models.

However, irradiance monitoring and performance testing in bifacial systems are complicated by the nonuniform nature of rear-side irradiance on the active surfaces, among other factors [4], [5]. Uncertainty in the ability of performance tests to accurately assess bifacial output can lead to questions during the commissioning of a new PV system and can adversely impact project economics depending on seasonality and changing ground conditions. Apparent bifacial system under-performance could actually be due to errors in the simulation model or uncertainty in quantifying dynamic rear-side irradiance contributions. Or there may actually be a problem in the construction or design of the system.

To address these questions, in this work, we evaluate various possible protocols and their impact on uncertainties in typical system performance metrics using one year of field test data. Our aim is to provide guidance to PV system designers, to be used when selecting irradiance measurement protocols for their bifacial systems.

The International Electrotechnical Commission (IEC) 61724-1 standard [8] defines requirements for PV performance monitoring and is widely followed worldwide. In 2021, this standard introduced requirements for bifacial systems, providing two options for quantifying rear plane-of-array (POA) irradiance. In option 1, rear POA irradiance is estimated from other measurements, using a view factor or raytracing model built into performance modeling software. In option 2, rear POA irradiance is directly measured, as illustrated in Fig. 1. In this work, we compare both options, using the performance ratio (PR) and capacity test ratio (CTR) as metrics.

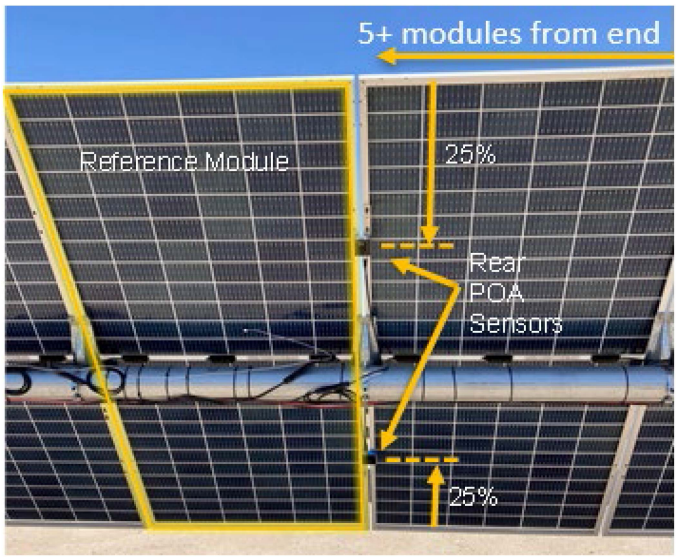

Fig. 1. Rear POA irradiance measurement examples, with requirements for irradiance sensor layout discussed in the current study. (Image courtesy of EDF).

One of the most widely used system metrics is the PR, also defined by IEC 61724-1, which compares measured energy to energy expected based on POA irradiance over a reporting period. With various slightly modified definitions, PR is often used worldwide for contractual assessments of system performance on a monthly or yearly basis. IEC 61724-1 contains a specific definition of PR for bifacial systems, which we analyze here.

Another widely used test, especially in the United States, is the capacity test, typically performed upon the completion of construction to confirm proper system operation. In the ASTM E2848 [9] capacity evaluation method, which is the most widely used, the measured system power output and the expected power output based on the performance model are each regressed to a common reporting condition and then compared to provide what is termed as a CTR. The currently published version of the standard does not contemplate bifacial systems, but the method can be easily modified for bifacial systems by adding the rear POA (G_{rear}) irradiance, weighted by the bifaciality factor φ, to the front POA (G_{front}) irradiance and using this sum in the regression equations in place of the front POA [10], [11]. This effective bifacial irradiance value is termed G_{total}:

$$G_{\mathrm{total}} = G_{\mathrm{front}} + \varphi \cdot G_{\mathrm{rear}}. \tag{1}$$

IEC 61724-2 [12] is another method for PV system capacity evaluation that is similar in intent to ASTM E2848 but follows different principles. In IEC 61724-2, instead of regressing system power output to a reporting condition, measured and expected system power outputs are directly compared at the test conditions. The currently published edition of IEC 61724-2 does not address bifacial systems, but a new edition draft is underway, which does address bifacial systems.

Excerpts are included herein which are used in our analysis.

We use the performance metrics discussed above—PR by IEC 61724-1, capacity ratio by ASTM E2848, and capacity ratio by IEC 61724-2—to examine the impacts of using different methods to quantify rear-side irradiance, including methods corresponding to IEC 61724-1 bifacial option 1 (model-based estimation) or option 2 (direct measurement) and subvariants of these options. To compare the methods and assess variability in the results due to weather, we calculate each performance metric weekly throughout a full year of data collection, while also comparing results to a baseline for a comparable monofacial system. The results allow us to identify potential uncertainties and tradeoffs associated with the different methods.

TABLE I
IRRADIANCE INSTRUMENTATION FOR EACH METHOD ANALYZED IN THIS WORK

Method	System	IEC 61724-1 Bifacial Instrumentation Category	Measured Irradiance					
			GHI	DHI and/or DNI	Albedo	Front POA (G_{front})	Rear POA (G_{rear})	Total POA
Baseline	Monofacial or Bifacial	n/a				o		
1	Bifacial	Opt. 1	o	o	o	o		
2A	Bifacial	Opt. 2				o	o	
2B	Bifacial	Opt. 2*				o^		o

*IEC-61724-1 does not mention reference modules for bifacial option 2, but they are analogous to rear-side reference cells in this context. ^For calibration of the reference module.

II. MEASUREMENT METHODS

A. Instrumentation Requirements

Our study follows and expands on the instrumentation requirements for fielded PV systems provided in IEC 61724-1. System power data and meteorological data, including temperature and irradiance, are required to assess field performance. In addition, rear-side irradiance contributions must be determined for bifacial systems.

We compare three different instrumentation options for quantifying rear-side irradiance, listed in Table I, as well as a baseline method designed for traditional monofacial systems in which only the front-side resource is collected.

In Method 1, a broadband albedometer on similar terrain to the array together with site-measured global horizontal irradiance (GHI) and diffuse horizontal irradiance (DHI) yields expected rear POA irradiance via a view-factor model [13], [14], [15], as specified in IEC 61724-1 bifacial option 1. Although IEC

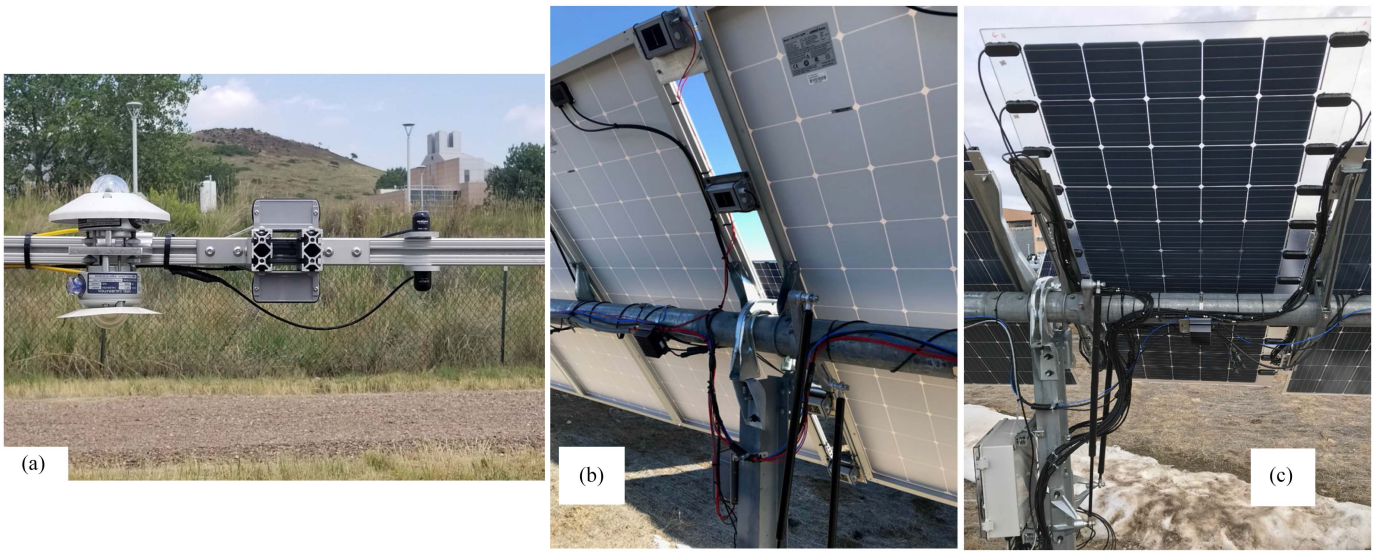

Fig. 2. Irradiance measurement instruments for rear-side resource at the bifacial experimental single-axis tracking (BEST) experiment at NREL. (a) Method 1 albedometer (broadband CM11 was used here). (b) Plane of array reference cells. (c) Custom bifacial reference module.

61724-1 lists the measurement of DHI as "optional," we have included the measurement of DHI in our analysis to achieve higher accuracy, and strongly recommend others to do the same.

In Method 2A, field-deployed rear-facing POA reference cells (or, optionally, broadband pyranometers) directly measure rear irradiance, G_{rear}, as specified in IEC 61724-1 bifacial option 2. A similar concept is explored in Method 2B by using bifacial reference modules to directly measure G_{total} from a reference module's short-circuit current (I_{sc}) and temperature [16], [17]. Although IEC 61724-1 does not mention reference modules, we consider this a variant of IEC 61724-1 bifacial option 2 because rear irradiance (specifically G_{total}) is directly measured rather than modeled.

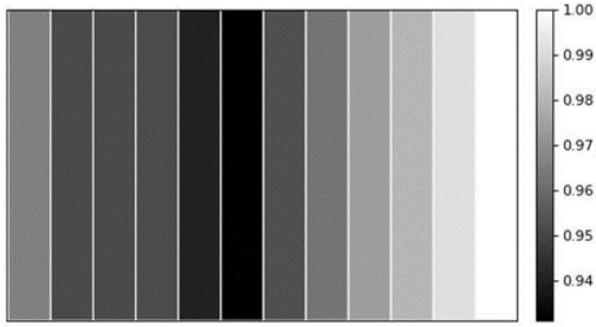

Fig. 3. Relative bifacial current of the 12-channel reference module of Fig. 2 over two months of measurement. Torque-tube shading is visible in the middle of the module and increased ground-reflected irradiance is visible at the ends.

B. Rear POA Sensor Positions

IEC 61724-1 directs that rear POA sensors should be placed in locations where they will receive irradiance representative of the average rear POA, but while the currently published 2021 edition provides some guidance, it does not specify these locations. A primary consideration for rear irradiance nonuniformity is the natural variability across the chord of a bifacial module due to ground reflections, diffuse irradiance collection, and the structure shading. A second consideration is edge brightening at the ends of rows due to proximity to unshaded areas of the field. Both are crucial factors in the analysis of bifacial system performance [11], [18], [19], [20], [21], [22], [38].

To evaluate the first effect, we have employed a custom reference module, shown in Fig. 2(c). Unlike a conventional module, this custom glass–glass module has cells strung horizontally across the short axis of the module and contacted at each end, creating 12 individually addressed substrings of bifacial cells. This allows us to measure the natural spatial variability of bifacial irradiance, and assess the ideal placement of a combination of rear irradiance sensors. Fig. 3 shows 2 months of cumulative current measurement for each of the 12 individual channels to illustrate the bifacial irradiance gradient. To evaluate the ideal placement of two hypothetical irradiance sensors, we have taken each possible substring pair and averaged their current measurements for two years of data. Comparing the RMSE relative to the overall average current across the module indicates that RMSE is minimized for the two substrings positioned at 25% and 75% from the module edge [23], [24]. This is in agreement with other studies for different PV array configurations [25], [26].

For the second effect of edge brightening, we propose a simplified method to calculate the minimal distance from the edge for rear POA irradiance sensors to avoid edge effects, as illustrated in Fig. 4. Considering a bifacial north–south single-axis tracking system, we require that rear POA sensors be placed at least a distance from the edge d, as defined in (2). Here, α is the angle between the rear sensor and the position of the maximum extent of ground illumination at solar noon during the winter solstice, marking the sun's lowest annual elevation in the sky.

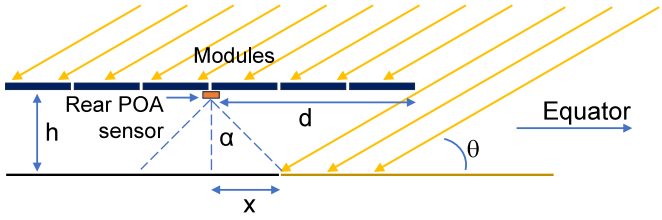

Fig. 4. Ground illumination under equator-end modules in single-axis trackers, showing rear POA sensor distance for minimal edge effects. Modules pictured at noon.

TABLE II
LATITUDE AND HUB-HEIGHT RELATIONSHIP TO REAR POA SENSOR PLACEMENT FOR AVOIDING EDGE EFFECTS

Latitude	Min. solar elevation at noon in winter (degrees)	Recommended minimum distance from edge for various hub heights		
		Height 1.25 m	Height 1.5 m	Height 2 m
±20°	47	2.0 m	2.4 m	3.2 m
±40°	27	3.3 m	3.9 m	5.3 m
±50°	17	4.9 m	5.9 m	7.9 m

This represents the sensor's view angle, which ideally includes a minimum of the illuminated ground at the end. Using this requirement, the minimum allowed distance d from the edge for rear POA irradiance sensors and reference modules is

$$d = \frac{h}{\tan\theta} + \frac{h}{\tan\alpha} = h\left(\frac{1}{\tan\theta} + \frac{1}{\tan\alpha}\right) \tag{2}$$

where h is the tracker's torque-tube height in meters and θ is the minimum annual solar elevation angle at solar noon. Results for some latitudes and height cases are shown in Table II, in each case choosing d to achieve $<7\%$ error in measured G_{Rear} from the contribution of end ground illumination. For the analysis in Table II, we assume a diffuse fraction of 0.2 and ground coverage ratio (GCR) of 0.3. Based on this analysis, we make a general recommendation to place rear-side irradiance sensors at least 5 m from the equator-facing end of a row to avoid edge effects in most systems. This is also in agreement with more detailed analyses of edge effects performed using ray-tracing models [4], [11], [18] and field measurements [23]. Note that while the recommendation is derived specifically for the end of a north–south oriented tracker row closest to the equator (e.g., the south end of a tracker sited in the northern hemisphere), the recommendation may also be used for the opposite end and even for fixed-tilt systems, as these have lesser requirements for avoidance of edge effects during the primary power-producing hours of the day.

Our rear POA sensor placements in this study follow the above recommendations for bifacial single-axis tracking arrays.

C. Field Data Collection

Field performance data for this study comes from the 75-kW BEST field at NREL [27]. The entire site is composed of 10 single-axis tracker rows, in one-module-portrait ("1P") configuration with a 0.35 GCR. This field has module-level and string-level data for five rows of different bifacial technologies and their comparison monofacial rows, and it is also instrumented with different types of G_{front}, G_{rear}, albedo, module temperature, and weather sensors. Data captured since 2019 is made publicly available by the authors for use by other researchers.

Field testing for this experiment ran from June 2021 through May 2022, with string-level dc data forming the basis for the measured system performance. AcuDC power meters with 0.5% accuracy class were used, with data averaged over 5-min periods.

For this experiment, two effective PV systems were compared: one monofacial system comprising a single row of 20 PERC monofacial modules (Row 8, 7.2 kWdc), and another that combined the power of two PERC bifacial rows (Rows 2 & 4, 13.9 kWdc). Per-module dc–dc power optimizers were used as part of the system's grid interconnection (SolarEdge P505).

The site was equipped with a full range of meteorological instrumentation, summarized in Table I, including ambient temperature and wind speed, along with ground albedo measurements from a horizontal CM-11 albedometer. Front POA irradiance (G_{front}) was measured with a broadband pyranometer, calibrated to have an absolute accuracy of 3% at 1000 W/m^2 and normal incidence. The G_{front} sensor was placed on a tracker row in an unshaded location near the center of rotation of the modules, and the front POA sensor followed the same tracked angle throughout the day as the rest of the field.

Rear irradiance for Method 2A was measured by an average of four rear-facing, temperature-corrected reference cells (IMT model Si-01). To gather spatial variability across the module length, these were distributed along a module as shown in Fig. 2, at spacings roughly 0%, 25%, 75%, and 100% across the module plane. For more typical applications of this method, it would be sufficient to use two reference cells at 25% and 75% positions along the module as discussed above.

Rear irradiance for Method 2B was collected with a custom bifacial reference module, shown in Fig. 2. As described previously, this custom glass–glass module has 12 individually contacted substrings of bifacial cells. An average of temperature-corrected I_{sc} was taken over all substrings to directly obtain the effective bifacial irradiance, G_{total} for the reference module. For the easier application of this method, any bifacial module in the array could be used as a reference module, and the G_{total} obtained from that module's I_{sc}, e.g., with an *in situ* curve-tracing unit [5], [16], [25] or monitoring over a current shunt.

Site weather data were measured by the nearby (<1 km) Solar Radiation Research Laboratory [28], including GHI from a CMP-22 horizontal pyranometer and DHI from a shaded CM-22 pyranometer.

D. Reference Module Field Calibration

For the reference module in Method 2B, a direct field calibration was conducted for front-side-only module power output by covering the module's rear side with a black cloth. Five-minute

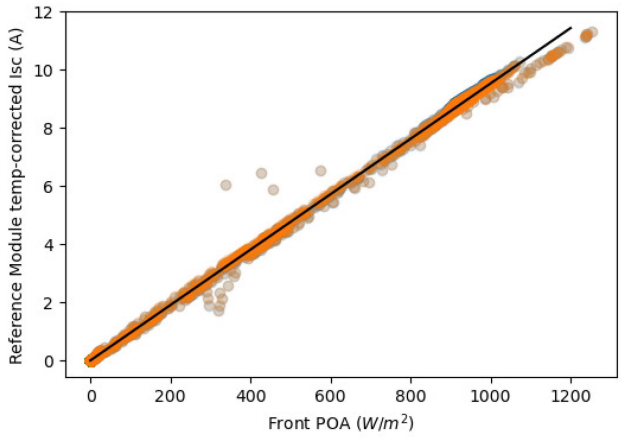

Fig. 5. Calibration of the reference module against the front POA sensor with the rear of the reference module covered. Field calibration reduces bias error for Method 2B.

data were collected over two sunny days, and a linear regression was performed for the reference module's temperature-corrected I_{sc} against the broadband pyranometer's G_{front}, as shown in Fig. 5, yielding a calibration coefficient for one-sun front-only I_{sc}. Afterward, the rear was uncovered and total temperature-corrected I_{sc} was measured and used with the calibration coefficient to determine the total front and rear irradiance G_{total}. This addresses calibration differences which could introduce bias error between the bifacial reference module and the more accurate pyranometer. In this case, a difference of 2.3% was found between nameplate and field-calibrated $I_{sc,}$ which is a sizeable difference.

III. Analysis Methods

Three methods of analysis for initial system performance are considered here—PR, ASTM E2848 capacity test, and IEC 61724-2 capacity test. We investigated each of these analysis methods along with each of our three instrumentation options. Because initial acceptance testing is expected to be conducted in a short period of time, our 1-year dataset is divided into weekly segments, and performance methods are conducted independently on each weekly segment. Further method details are provided further.

A. PR Calculation

PR represents measured energy production divided by expected energy production, where expected energy is based simply on the irradiance-weighted temperature-corrected-power integrated over a given time. Here, we use two modified equations for PR given in IEC 61724-1:2021 section 14, which include temperature-corrected PR for monofacial systems and temperature-corrected PR for bifacial systems which includes rear POA irradiance in the expected energy calculation, using a bifacial irradiance factor (BIF). IEC 61724-1 defines BIF as

$$\mathrm{BIF} = 1 + \varphi \cdot \frac{G_{\mathrm{rear}}}{G_{\mathrm{front}}}. \tag{3}$$

In this work, we determined BIF according to each of the rear irradiance methods in Table I, as explained further below. We used the annual-temperature-equivalent PR equation including BIF (Eq. 29 in IEC 61724-1) given by

$$\mathrm{PR}_{\mathrm{BIF}} = \sum P / \sum \frac{C \times P_0 \times G_{\mathrm{front}} \times \mathrm{BIF}}{1000\ \mathrm{W/m^2}} \tag{4}$$

where P is the system ac power output, P_0 is the system dc power rating at STC. C is a temperature correction factor that corrects expected power at each time point for the difference between the instantaneous temperature and an annual average temperature and is given by

$$C = 1 + \gamma \times (T - T_{\mathrm{annual-avg}}) \tag{5}$$

where γ is the PV temperature-coefficient of power, T is the PV cell temperature, and $T_{\mathrm{annual\text{-}avg}}$ is the annual-average PV cell temperature. Setting BIF to 1 in (4) reduces it to the monofacial version of the annual-temperature-equivalent PR equation (Eq. 26 in IEC 61724-1)

$$PR_{\mathrm{Mono}} = \sum P / \sum \frac{C \times P_0 \times G_{\mathrm{front}}}{1000\ \mathrm{W/m^2}}. \tag{6}$$

Although the PR equation for bifacial systems includes bifacial rear contribution through the BIF, it is not always desired to incorporate the rear irradiance contribution when calculating PR. Including the BIF correction makes the PR result less sensitive to changes in ground albedo, and therefore more useful in capacity test applications. However, this can sometimes lead to confusion in assuming that the bifacial system is not performing any better than a comparison monofacial system, despite having greater energy yield [29]. For this reason, we calculate PR as either the bifacial or monofacial formulation to illustrate the difference.

To present PR results that are consistent with the other methods considered here, irradiance conditions are filtered for $G_{\mathrm{front}} > 400\ \mathrm{Wm^{-2}}$ and a Hampel outlier filter excludes points 5σ away from the mean in a given 7-day window [30].

B. ASTM E2848 Capacity Test Method

Our ASTM E2848 capacity test methodology largely follows the ASTM E2848-13(2018) standard, but we use different input variables for each rear irradiance method used. Previous suggestions for bifacial modifications of capacity testing procedures given in [10] have informed our approach.

ASTM E2848 provides a regression equation for relating system output power P to weather conditions

$$P = G \times (a_1 + a_2 G + a_3 T_{\mathrm{amb}} + a_4 v) \tag{7}$$

where G is POA irradiance, T_{amb} is ambient temperature, v is wind speed, and $a_1 - a_4$ are constants used to fit the relationship between power and meteorological conditions. Separate multilinear regressions are performed for both measured and modeled data, and then power is compared at a common reporting condition to compute a CTR:

$$\mathrm{CTR} = P_R^{\mathrm{measured}} / P_R^{\mathrm{modeled}} \tag{8}$$

TABLE III
ASTM E2848 CAPACITY TEST INPUT VARIABLES FOR EACH METHOD

Method	Modeled Regression (Hourly average)		Measured Regression (15-min average)		Reporting Condition
	G Irradiance	P Power	G Irradiance	P Power	
Baseline (monofacial and bifacial)	G_{front} modeled based on historical weather data (NSRDB 2020), using DNI, DHI, albedo	Modeled power, from System Advisor Model (SAM), using historical weather data	Measured G_{front}	Measured power	Determined by PV CapTest defaults, based on ASTM E2939: 60th percentile of measured irradiance
1	G_{front} modeled based on field-measured GHI, albedo, and DHI	Modeled power, from SAM bifacial model with hourly field-measured albedo			
2A	G_{total} modeled from G_{front} and G_{rear}, where $G_{total} = G_{front} + \phi * G_{rear}$ Based on historical DNI, DHI, albedo weather data	Modeled power, from SAM bifacial model	G_{total} = measured front $G_{front} + \phi * G_{rear}$	Measured power	
2B			G_{total} = measured G_{total} with reference module, calibrated		

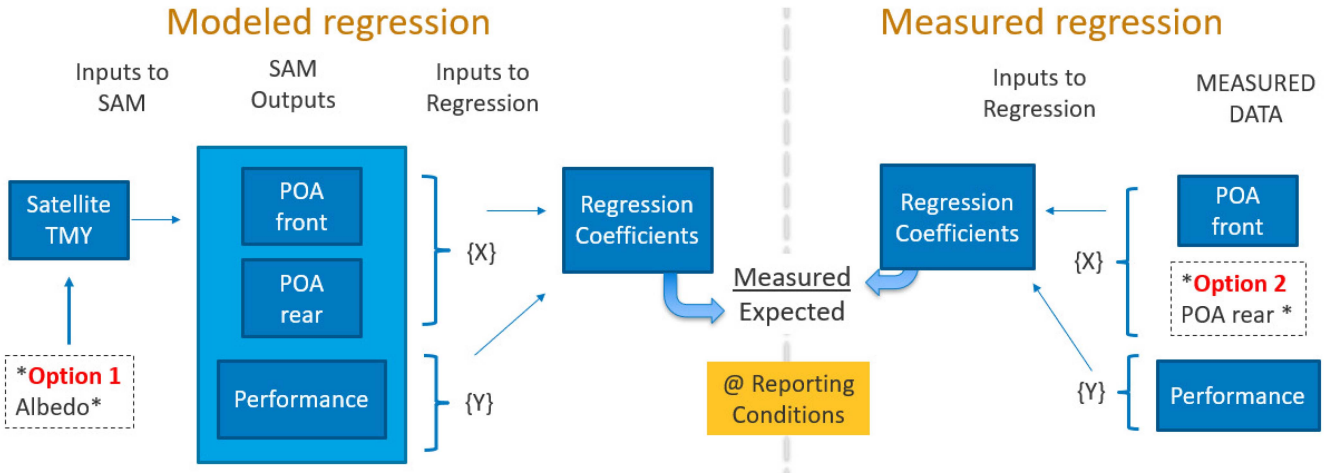

Fig. 6. Flowchart diagram of the ASTM E2848 capacity test analysis.

where $P_R^{measured}$ is the value of the measured power regression at the reporting condition and $P_R^{modeled}$ is the value of the modeled power regression at the reporting condition.

We use various formulations to calculate G and P in (7) to test the different rear irradiance instrumentation methods. Details of these formulations are listed in Table III, and the ASTM approach is further illustrated in Fig. 6. In Method 1 where rear POA measurements are not used, we replace G in (7) with G_{front}, the front POA irradiance. For modeled power P, we use the performance model software which includes the effects of both front and rear irradiance, with rear irradiance modeled based on the irradiance inputs listed in Table III. In Method 2A, we replace front-only G in (7) with $G_{total,}$ by including measured rear irradiance as suggested in [10]. Specifically, G_{total} is measured per (1) where φ is the modules' bifaciality factor (0.72 flash-tested value) and G_{rear} is the average of our four rear POA sensor measurements.

In Method 2B, the measured G_{total} is determined directly from a bifacial reference module, as discussed above.

The capacity test analysis was implemented in the PVCaptest Python software [31], [32]. Following the recommendations of ASTM E2939-2013, we filtered the hourly values and then

calculated monthly reporting conditions as the 60th percentile of irradiance along with mean ambient temperature and mean windspeed.

To conduct the regression and capacity test, we divided measured and modeled data into weekly segments, with each week representing a separate test result. Outlier, irradiance, and linearity filtering were conducted per ASTM E2848 using PVCaptest default values.

C. ASTM E2848 System Performance Model

Modeled system performance data comes from SAM [5] simulation. For the model input, the power rating of each row was determined by indoor *I-V* flash characterization of each module in the row plus application of a field degradation term of 0.6%–1.7% following remeasurement of a subset of modules at the end of the test period. The time series of expected performance for the ASTM method was calculated based on TMY weather data obtained from the National Solar Radiation Database (NSRDB) [33]. This follows the ASTM approach which uses a separate multivariate regression for modeled and measured data. Therefore, there is no need for the model weather file to match what was seen during the capacity test period. Here hourly-averaged TMY data for DNI, GHI, DHI, ambient temperature, and windspeed are used in the California Energy Commission's five-parameter performance model as implemented by SAM to determine the hourly dc output power.

For our initial modeling run of the baseline monofacial system, cumulative energy was found to be within ∼4% of the actual field-measured output for the monofacial system (row 8). Because the purpose of this study was not to investigate the absolute accuracy of performance models for monofacial systems, but instead to focus on the differences between the various bifacial instrumentation approaches, an empirical dc loss factor of 4.1% was introduced for all simulations. This has the effect of zeroing out the mean bias deviation (MBD) for the monofacial system and presenting each of the other methods as relative differences to this baseline case.

We consider our 4.1% empirical adjustment to be justified because this loss factor was applied across all simulation scenarios, both monofacial and bifacial. It is also a realistic value because there is a range of factors not otherwise accounted for in the simulation, such as cable resistive loss, soiling, and module-level converter efficiency. Additional sources of bias that may also contribute to this empirical factor include error in the transposition of irradiance from DNI/GHI to POA [34], [35] and broadband pyranometer uncertainty, which increases at low irradiance and high incidence angle [36], [37]. These all factors could contribute to the overall bias of predicted versus actual output, which we are attempting to correct in the case of the monofacial baseline.

D. IEC 61724-2 Capacity Test Method

The IEC 61724-2 capacity test method differs from the ASTM E2848 method in that, rather than regressing the measured and modeled system power to a reporting condition for comparison, the measured and modeled power are directly compared at the conditions of the test. The test method, originally published in 2016, is currently being revised to edition 2, and here we use and summarize this still-unpublished draft copy. The draft defines the test result as the power performance index (PPI):

$$\text{PPI} = \frac{\sum_i P_i^{\text{measured}}}{\sum_i P_i^{\text{expected}}} \tag{9}$$

where P_i^{measured} and P_i^{expected} are the measured and expected system power at each time interval i. Per the draft document, the data used for the sums in (9) are filtered to include only time intervals with POA irradiance >400 W/m^2 and to exclude any intervals with inverter clipping. The draft suggests the use of an outlier filter on instantaneous PPI, and here we employ a Hampel filter with a window of 7 days and passband of 5σ. This results in an exclusion of only 8% of datapoints, mostly under variable irradiance conditions.

The draft document requires a data recording interval of 1 min, but here we averaged to 5-min data due to difficulties performing 1-min modeling with SAM over the extended data set.

TABLE IV
IEC 61724-2 PERFORMANCE MODEL VARIABLES

Method	Model Input and Response (5-min average)	
	G Irradiance input	P Power response
Baseline (monofacial)	Field-measured GHI, DHI, albedo	SAM monofacial model
1	Field-measured GHI, DHI, albedo	SAM bifacial model
2A	G_{total} = measured front G_{front} + ϕ* G_{rear}	SAM **monofacial** model
2B	G_{total} = measured reference module I_{sc} calibrated & temp. corrected	

E. IEC 61724-2 System Performance Model

The expected power in the denominator of (9) in the IEC 61724-2 capacity test method is modeled by SAM, similarly to the ASTM method. However, rather than using TMY data for weather conditions, the IEC method requires expected power to be based on the field-measured weather data corresponding to the field performance data at each time interval. Here we use 5-min-averaged weather data from the met station described in Section II-C. Table IV provides details on the performance modeling analysis for the IEC test method for each of the instrumentation options. In the case of Methods 2A or 2B, as called for in the draft standard, measured G_{total} is passed to the model instead of G_{front} input irradiance. Also, as specified

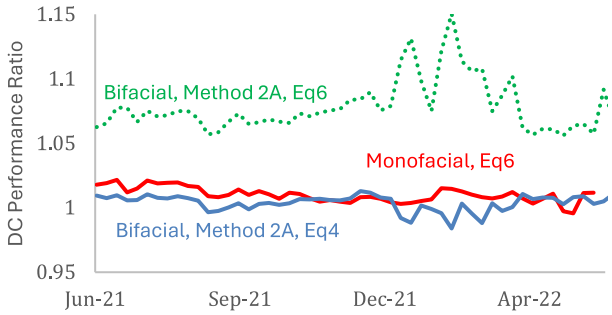

Fig. 7. Temperature-corrected dc PR for monofacial and bifacial systems. Bifacial system PR can either correct for rear irradiance contribution [BIF correction, (4)] or compare directly against monofacial systems using the standard monofacial equation (6).

in the document, a monofacial model is selected for the SAM simulation for Method 2. This is because G_{total} already adjusts for the increased apparent irradiance of a bifacial module along with its bifaciality factor. Only in the case of Method 1 which does not include measured G_{rear} is the SAM view-factor bifacial irradiance model invoked.

As with the case of the ASTM analysis, a 4.1% empirical loss factor is applied to the SAM modeled results, to reduce the MBD of the monofacial baseline.

IV. Results

A. PR Results

Fig. 7 compares the results of the temperature-corrected dc PR calculations, using the standard monofacial equation (6) and the BIF-corrected bifacial equation (4). Beginning with the monofacial system [Monofacial, equation (6), red solid line], we see that the PR values are close to 1.0. Such a high PR is somewhat unexpected, but can be explained by the fact that these are temperature-corrected, dc PR. The more common uncorrected ac PR values are typically lower due to the inclusion of inverter efficiency and temperature coefficient losses. We are also filtering for external conditions that may impact PR, such as low irradiance, partial shading, backtracking, or system outage.

For the bifacial system, we can calculate PR using two different equations, depending on whether rear irradiance is included with the incident POA resource or not. If we use the bifacial-irradiance-factor corrected PR (4), it gives PR values close to that of the monofacial baseline, around 1.0. Although the overall energy yield for the bifacial strings is around 6%–7% higher due to the bifacial energy gain, the use of (4) results in equivalent PR close to the monofacial baseline. This is because the BIF compensation includes measured G_{rear} in the denominator, and therefore, corrects for this additional bifacial resource.

When we instead compare the trace using the non-BIF corrected equation [Method 2A (6), green dotted], the PR is higher than the monofacial baseline by 7% on average. This is because the standard PR calculation is based only on the front-side POA irradiance; the additional bifacial energy generation is not offset by including rear-side irradiance in the denominator. Bifacial gain was highest in winter months (January–March, 2022) because of snow elevating ground albedo, and the uncorrected PR shows these variations.

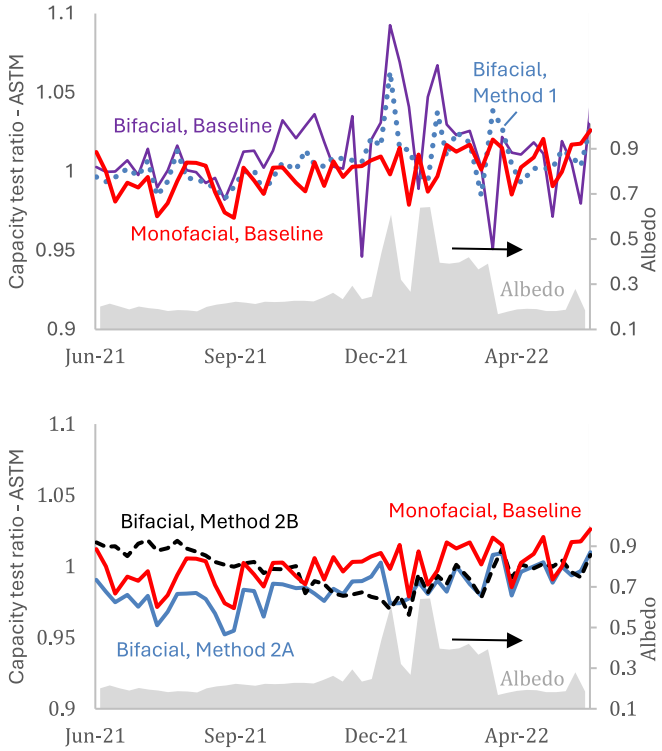

Fig. 8. CTR (measured/modeled) per ASTM E2848 for 52 separate 1-week intervals. Top panel: Monofacial (red) versus bifacial analyzed with front POA only (baseline, purple) and Method 1 (blue dotted). Measured ground albedo is shown on the second axis in gray on both panels. Bottom panel: Bifacial analyzed with Method 2A rear-facing reference cell (blue) and Method 2B bifacial reference module (black dashed). Monofacial baseline is shown in red.

When using the PR equations in 61724-1 for bifacial systems, the non-BIF corrected equation (6) should be used when you want to reflect the additional bifacial energy gain of the system. When used as a capacity test, the BIF-corrected bifacial PR (4) can be useful because PR values will be corrected for variable ground albedo and will remain more consistent.

B. ASTM E2848 Capacity Test Results

Fig. 8 presents the results of the ASTM E2848 CTR analysis using the different regression methods listed in Table III. For clarity, the comparison of the different methods is spread across two panels in the figure. Results for the monofacial baseline system, in red, are shown identically on both panels.

Results shown in Fig. 8 for the bifacial baseline method and Method 1 show the greatest variability, especially during winter months (December–March) with high albedo due to snow cover. In the case of the baseline method, historical TMY ground albedo values were used for the model regression instead of field-measured values. Assumed and actual albedo values were clearly mismatched for this case, resulting in large discrepancies in actual versus expected bifacial performance regression,

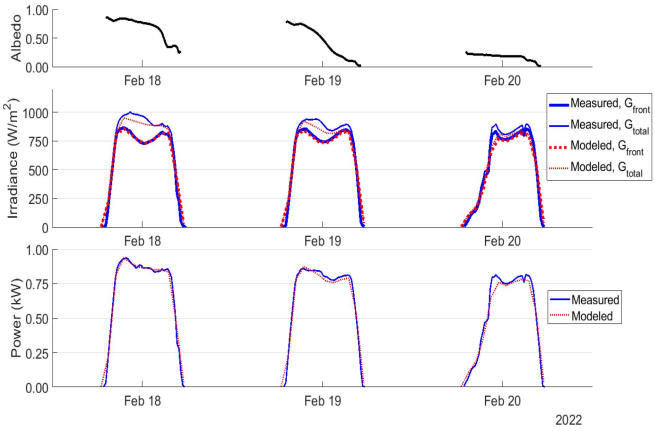

Fig. 9. Time series plot of representative data illustrating the effect of varying albedo (due to melting snow cover) on measured (blue) and modeled (red) power and G_{total} versus G_{front}.

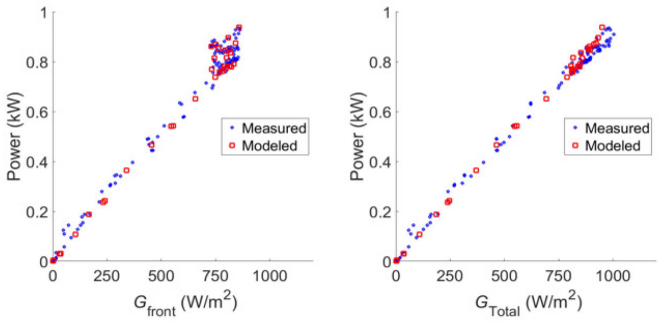

Fig. 10. Measured (blue, closed) and modeled (red, open) bifacial row four power versus irradiance for three sunny days with large albedo variations due to snow cover beginning 18 February 2022, showing correlation of power with G_{front} as in Method 1 (left), versus G_{total} as in Method 2 (right).

including large spikes in performance when field albedo was low, but historical TMY albedo was high.

Even Method 1—which uses a performance model that is corrected for field-measured albedo, GHI, and DHI—shows significant variability during winter months. This can be explained by a reduction in the quality of the regression when G_{front} is used as the only irradiance quantity. This is a necessity of the method because G_{rear} is not a measured quantity for Method 1.

Figs. 9 and 10 illustrate this point using data from a three-day period with significantly varying albedo due to melting snow cover. As shown in Fig. 9, the system performance model, using measured albedo, correctly predicts the system power. However, as shown in Fig. 10 (left plot), when system power is plotted against G_{front}, there is a cluster of points at high irradiance, which can result in poor fits in the E2848 CTR calculation. One reason for the variability of results in this situation is that the filtering steps prescribed by the E2848 regression method may selectively remove points in the cluster region, leading to a deviation between measured and modeled regressions. The order of filtering steps may also affect the results. However, this cluster disappears when the system power is plotted against G_{total}, leading to more stable results, as shown below.

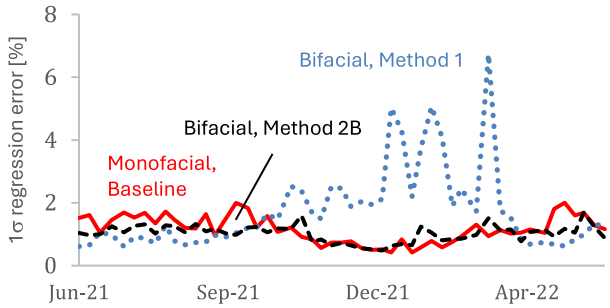

Fig. 11. Regression error from the ASTM fit to model data. Monofacial method (red) versus bifacial method 1 (blue dotted) and bifacial Method 2B (black dashed).

The lower panel of Fig. 8 shows the CTR results using Method 2A and 2B, where rear irradiance is explicitly measured and the capacity test is calculated using G_{total} per Table III. This figure panel shows greatly reduced variations in the CTR result for these cases.

Fig. 11 further illustrates the improvement in the stability of the ASTM capacity test results when using methods based on regression against G_{total}. In this figure, we show the 1σ error for the multilinear regression assessed each week at the model reference conditions. The figure shows that the linear regression error of the weekly fits is as high as 6%–7% for Method 1 during times of high albedo, but is below 2% for Methods 2A (not shown) and 2B. When rear irradiance is not considered in the ASTM regression, unsatisfactory results are obtained, even if the overall power model accuracy is good.

Table V tabulates the weekly root mean square deviation (RMSD) and MBD in CTR results using each of the methods. Minimum and maximum CTRs determined for the year are also provided to give context on the ability of each method to successfully pass or fail under variable annual conditions. Note that typical contracts require a CTR above 0.95 or 0.97, i.e., only allowing a 3%–5% margin of error. Systematic variations in the CTR testing exceeding this value could, therefore, cause difficulties in commissioning bifacial PV systems under standard commercial agreements which account for bifacial gains in the contractual performance model. Conversely, uncorrected overperformance during periods of snow and high albedo could mask underlying performance issues which would pass risk on to the system purchaser. Either using rear irradiance measurement (Methods 2A or 2B) or restricting the analysis to periods with less albedo variation (in this case, periods without snow) reduces the variation, and ultimately the uncertainty in performance testing. In either case, the variability of the capacity test for bifacial systems can be made comparable to that of the monofacial system.

C. IEC 61724-2 Capacity Test Results

Results of the IEC 61724-2 capacity test analysis are presented in Fig. 12 with their statistics also summarized in Table V. Results of the monofacial analysis were qualitatively similar to those for the ASTM E2848 analysis, with comparable mean

TABLE V
ANNUAL VARIANCE OF EACH CAPACITY TEST APPROACH

System	Method	ASTM E2848				IEC 61724-2			
		MBD [%]	RMSD [%]	MIN [frac]	MAX [frac]	MBD [%]	RMSD [%]	MIN [frac]	MAX [frac]
Monofacial	Monofacial Baseline	0.0	1.3	0.97	1.03	0.0	1.2	0.96	1.03
Bifacial	Bifacial Baseline	1.3	2.6	0.95	1.09	-	-	-	-
Bifacial	1	0.6	1.5	0.98	1.06	0.7	0.9	0.99	1.02
Bifacial	2A	−1.6	1.3	0.95	1.01	−1.1	0.9	0.97	1.01
Bifacial	2B	−0.3	1.3	0.97	1.02	0.9	0.8	1.00	1.03

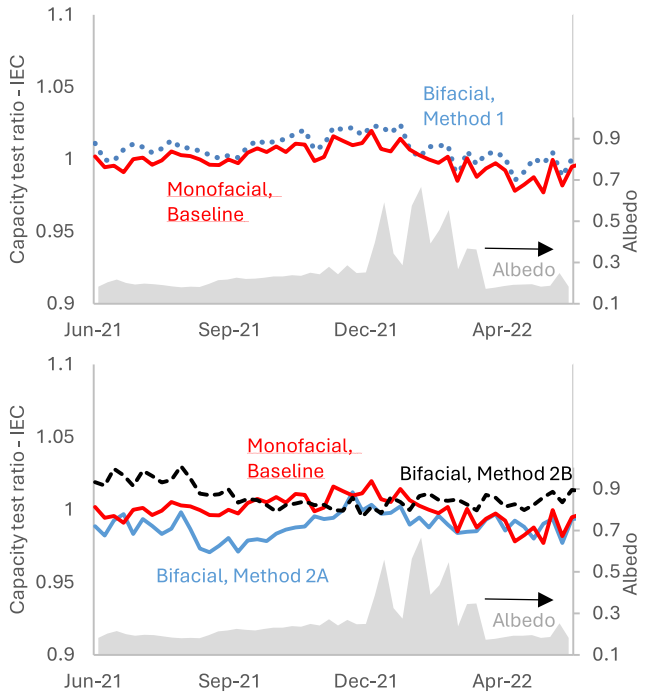

Fig. 12. CTR (measured/modeled) per IEC 61724-2 (second edition draft) for 52 separate 1-week intervals. Top panel: Monofacial (red) versus bifacial analyzed with GHI and DHI (Method 1, blue dashed). The measured ground albedo is shown on the second axis in gray on both panels. Bottom panel: Bifacial analyzed with Method 2A rear-facing reference cell (light blue) and Method 2B bifacial reference module (black dashed).

bias and RMS deviation. Compared with the ASTM approach, variability in the bifacial system capacity test is significantly lower, with RMSD reduced across the board when using the IEC 61724-2 process. In particular, for Method 1 which uses modeled G_{rear}, much lower variability is obtained using the IEC 61724-2 method, compared with the ASTM regression approach. Comparable performance is observed between the use of bifacial irradiance methods 2A (reference cell) and 2B (reference module).

V. DISCUSSION

Common commercial practices in the United States continue to rely primarily on capacity testing per ASTM E2848 to demonstrate bifacial PV plant performance postcommissioning. At present, these practices are rarely modified beyond the requirements that would be typical for monofacial systems with frontside-only irradiance measurements. This means that the expected bifacial gain is treated only as a bonus to the project performance and any shortfall in bifacial gain is not evaluated. Adding instrumentation to measure rear-side irradiance means that the system performance can be evaluated against total front and rear irradiance contributions.

However, the method of accounting for rear-side irradiance can lead to differences in risk apportionment and performance test results. In methodologies like Method 1, where rear irradiance is estimated using performance models from the initial system design, the engineering firm responsible for the design and construction of the site assumes the risk of any inaccuracies in modeling the performance of the rear side, rather than the project owner. However, this advantage is obtained at the cost of increased model complexity. When using methods such as 2A or 2B that directly measure rear irradiance, any shortfall in predicted rear irradiance is not evaluated, but potential module bifacial underperformance is evaluated. The application of Methods 2A and 2B is also simpler than the modeling required to carry out Method 1.

Comparing the various methods outlined above, the results of this work highlight that the CTR can be greatly influenced by changing ground conditions without measuring and accounting for it with measured G_{rear}. This is illustrated by the high variability seen in Fig. 8's bifacial baseline which is regressed

entirely on G_{front}. Actual ground-reflected irradiance can differ significantly from the original performance model, resulting in large volatility in the monitored PR, especially under high albedo conditions, such as snow.

The ASTM results presented above demonstrate the advantages of Methods 2A and 2B, which showed lower RMSD across the year-long campaign, particularly as compared to the baseline method (G_{front}) or Method 1 (modeled G_{rear}). A comparison of regression model errors identified that the root cause of much of the resulting RMSD in these methods is the uncertainty in the regression during times of high albedo (snowy periods).

By comparison, the IEC 61724-2 approach does not make use of multilinear regression and, therefore, provides improved stability with Method 1's modeled G_{rear}. Similar performance was obtained with the use of Method 2's measured G_{rear}, in the case of either measurement with rear-facing reference cells or reference modules.

Finally, any bias in the test results is also very important to the parties conducting a test. When using rear-side irradiance sensors, the sensor calibration must be accurate. When using a reference module to measure total front plus rear irradiance contributions, we advise checking the reference module calibration against front POA sensors as discussed above.

VI. Conclusion

Incorporating field-measured rear irradiance measurements improves the repeatability of bifacial CTR measurements, particularly during high and variable albedo conditions, as evidenced by the reduced standard deviations of repeated tests over a 1-year field study. This is important due to the tight tolerances required to pass a capacity test and ideally should return valid results under a wide range of environmental and ground albedo conditions.

The instrumentation standards outlined in IEC 61724-1:2021 include options for both measured and modeled system G_{rear}, both of which we have investigated here. When using the ASTM-E2848 method, incorporating measured (rather than modeled) G_{rear} yields the highest accuracy. Also, bifacial reference modules appear to be a viable option, so long as they are suitably calibrated against a front-facing low-error broadband pyranometer.

Other test methods were investigated, including PR and a new draft IEC 61724-2 capacity test, and they were found to also provide a good response for bifacial systems. In particular, there is some confusion about the new BIF-corrected PR in IEC 61724-1. A bifacial system can be evaluated using either the conventional PR equation or BIF-corrected PR. In the case of BIF correction, any apparent bifacial gain will be incorporated into the expected power, because the rear irradiance contribution is added to the resource in the denominator. Including the BIF correction makes the PR result less sensitive to changes in ground albedo, and therefore more useful in capacity test applications. However, this can sometimes lead to confusion—more energy is indeed being produced by the bifacial system, it is just being compared against a proportionally higher irradiance reference.

Overall, we found similar results between the capacity test methods. Under variable albedo conditions, measured G_{rear} is highly recommended. If Method 1 (modeled G_{rear} from measured albedo) instrumentation is desired, the draft IEC 61724-2 method provides superior results. In the case that the capacity test can be confined to times of constant low surface albedo, however, all approaches—even ASTM using front-only measurement and regression—could provide reasonable capacity test values.

Acknowledgment

The views expressed in the article do not necessarily represent the views of the DOE or the U.S. Government. The U.S. Government retains and the publisher, by accepting the article for publication, acknowledges that the U.S. Government retains a nonexclusive, paid-up, irrevocable, worldwide license to publish or reproduce the published form of this work, or allow others to do so, for U.S. Government purposes.

Competing interests: The authors have declared that no competing interests exist.

Data and Code Availability Statement: Performance and weather data used for the analysis can be downloaded from https://datahub.duramat.org/dataset/best-field-data.

Inclusion and Diversity: One or more of the authors of this paper self-identifies as an underrepresented ethnic minority in science. While citing references scientifically relevant for this work, we also actively worked to promote gender balance in our reference list.

References

[1] M. Fischer, "ITRPV 2024," PV CellTech, Frankfurt/Main, 2024. [Online]. Available: https://www.vdma.org/international-technology-roadmap-photovoltaic

[2] M. Wood, "US solar PV system pricing: H1 2022," Edinburgh, UK: Wood Mackenzie, Market Report, 2022.

[3] V. Ramasamy et al., "U.S. Solar photovoltaic system and energy storage cost benchmarks, with minimum sustainable price analysis: Q1 2023," NREL, Golden, CO, USA, Tech. Rep. NREL/TP-7A40-87303, Sep. 2023, doi: 10.2172/2005540.

[4] M. Topalov, "Challenges of bifacial module performance monitoring," PV Tech. Accessed: Dec. 08, 2023. [Online]. Available: https://www.pv-tech.org/challenges-of-bifacial-module-performance-monitoring/

[5] M. Gostein et al., "Measuring irradiance for bifacial PV systems," in *Proc. 2021 IEEE 48th Photovolt. Spec. Conf.*, 2021, pp. 0896–0903, doi: 10.1109/PVSC43889.2021.9518601.

[6] R. Kopecek and J. Libal, "Bifacial Photovoltaics 2021: Status, opportunities and challenges," *Energies*, vol. 14, no. 8, Apr. 2021, Art. no. 2076, doi: 10.3390/en14082076.

[7] J. S. Stein et al., "Bifacial photovoltaic modules and systems: Experience and results from international research and pilot applications," International Energy Agency, Paris, France, IEA-PVPS T13-14:2021, 2021. [Online]. Available: https://iea-pvps.org/wp-content/uploads/2021/04/IEA-PVPS-T13-14_2021-Bifacial-Photovoltaic-Modules-and-Systems-report.pdf

[8] *Photovoltaic System Performance–Part 1: Monitoring*, Standard IEC 61724-1:2021, IEC, Geneva, Switzerland, 2021. [Online]. Available: https://webstore.iec.ch/publication/65561

[9] ASTM, *Standard Test Method for Reporting Photovoltaic Non-concentrator System Performance*, Standard ASTM E2848-13, USA: ASTM, 2023.

[10] M. Waters, C. A. Deline, J. Kemnitz, and J. Webber, "Suggested modifications for bifacial capacity testing," in *Proc. 2019 IEEE 46th Photovolt. Spec. Conf.*, Golden, CO, USA, 2019, pp. 3519–3524, doi: 10.1109/PVSC40753.2019.9198974.

[11] C. Deline et al., "Assessment of bifacial photovoltaic module power rating methodologies—Inside and out," *IEEE J. Photovolt.*, vol. 7, no. 2, pp. 575–580, Mar. 2017, doi: 10.1109/JPHOTOV.2017.2650565.
[12] *Photovoltaic System Performance–Part 2: Capacity Evaluation Method*, Standard IEC TS 61724-2:2015, IEC, Geneva, Switzerland, 2016. [Online]. Available: https://webstore.iec.ch/publication/25982
[13] "System Advisor model version 2022.11.29," National Renewable Energy Laboratory, Golden, CO, USA. Accessed: Dec. 08, 2023. [Online]. Available: https://sam.nrel.gov
[14] NREL, "bifacialVF," GitHub, 2019. [Online]. Available: http://github.com/NREL/bifacialvf
[15] A. Mermoud and B. Wittmer, "Yield simulations for horizontal axis trackers with bifacial PV modules in PVsyst," in *Proc. EUPVSEC*, Brussels, Belgium, 2018, pp. 1929–1934.
[16] J. L. Braid et al., "Effective irradiance monitoring using reference modules," in *Proc. 2022 IEEE 49th Photovolt. Spec. Conf.*, Philadelphia, PA, USA, Jun. 2022, pp. 1073–1078, doi: 10.1109/PVSC48317.2022.9938851.
[17] J. Polo, M. Alonso-Abella, A. Marcos, C. Sanz-Saiz, and N. Martín-Chivelet, "On the use of reference modules in characterizing the performance of bifacial modules for rooftop canopy applications," *Renew. Energy*, vol. 220, Jan. 2024, Art. no. 119672, doi: 10.1016/j.renene.2023.119672.
[18] S. Ayala Pelaez, C. Deline, P. Greenberg, J. S. Stein, and R. K. Kostuk, "Model and validation of single-axis tracking with bifacial PV," *IEEE J. Photovolt.*, vol. 9, no. 3, pp. 715–721, May 2019, doi: 10.1109/JPHOTOV.2019.2892872.
[19] T. J. Coathup et al., "Impact of torque tube reflection on bifacial photovoltaic single axis tracked system performance," *Opt. Exp.*, vol. 31, no. 4, Feb. 2023, Art. no. 6143, doi: 10.1364/OE.481301.
[20] U. A. Yusufoglu et al., "Analysis of the annual performance of bifacial modules and optimization methods," *IEEE J. Photovolt.*, vol. 5, no. 1, pp. 320–328, Jan. 2015, doi: 10.1109/JPHOTOV.2014.2364406.
[21] K. R. McIntosh, M. D. Abbott, B. A. Sudbury, and J. Meydbray, "Mismatch loss in bifacial modules due to nonuniform illumination in 1-D tracking systems," *IEEE J. Photovolt.*, vol. 9, no. 6, pp. 1504–1512, Nov. 2019, doi: 10.1109/JPHOTOV.2019.2937217.
[22] K. R. McIntosh et al., "Irradiance on the upper and lower modules of a two-high bifacial tracking system," in *Proc. 2020 47th IEEE Photovolt. Spec. Conf.*, Jun. 2020, pp. 1916–1923, doi: 10.1109/PVSC45281.2020.9300838.
[23] S. Ovaitt et al., "Measuring and modeling bifacial technologies," in *Proc. bifiPV2022 Workshop*, Apr. 2022, Paper NREL/PR-5K00-82540. [Online]. Available: https://www.nrel.gov/docs/fy22osti/82540.pdf
[24] S. A. Pelaez et al., "Effect of torque-tube parameters on rear-irradiance and rear-shading loss for bifacial PV performance on single-axis tracking systems," in *Proc. 2019 46th Photovolt. Spec. Conf.*, Chicago, IL, USA, Jun. 2019, pp. 1–6, doi: 10.1109/PVSC40753.2019.9198975.
[25] M. Gostein, M. Bila, R. Campbell, P. Wolffersdorff, and J. Horst, "Soiling and irradiance measurements in bifacial PV systems using In-situ reference modules and rear-side reference cells," in *Proc. 40th Eur. Photovoltaic Sol. Energy Conf.*, 2023, pp. 1–3.
[26] N. Riedel-Lyngskar, M. Bartholomaus, J. Vedde, P. B. Poulsen, and S. Spataru, "Measuring irradiance with bifacial reference panels," *IEEE J. Photovolt.*, vol. 12, no. 6, pp. 1324–1333, Nov. 2022, doi: 10.1109/JPHOTOV.2022.3201468.
[27] S. Ovaitt, "BEST field data," DuraMAT Datahub, Sep. 30, 2022, doi: 10.21948/1787805.
[28] T. Stoffel and A. Andreas, "NREL solar radiation research laboratory (SRRL): Baseline measurement system (BMS)," National Renewable Energy Lab.(NREL), Golden, CO, USA, 1981, doi: 10.7799/1052221.
[29] E. Ogliari, A. Dolara, D. Mazzeo, G. Manzolini, and S. Leva, "Bifacial and monofacial PV systems performance assessment based on IEC 61724-1 standard," *IEEE J. Photovolt.*, vol. 13, no. 5, pp. 756–763, Sep. 2023, doi: 10.1109/JPHOTOV.2023.3295869.
[30] R. K. Pearson, Y. Neuvo, J. Astola, and M. Gabbouj, "Generalized Hampel filters," *EURASIP J. Adv. Signal Process.*, vol. 2016, no. 1, Dec. 2016, Art. no. 87, doi: 10.1186/s13634-016-0383-6.
[31] B. Taylor, K. Anderson, and C. Hansen, "pvcaptest: V0.10.0," Zenodo, Sep. 10, 2023, doi: 10.5281/zenodo.8332774.
[32] B. Taylor and J. Forbess, "captest: Open source package for reproducible performance testing," in *Proc. 12th PV Perform. Model. Workshop*, 2019, pp. 776–804, Accessed: Dec. 08, 2023. [Online]. Available: https://pvpmc.sandia.gov/workshops-and-pubs/workshops/2019-pvpmc-abq/
[33] M. Sengupta et al., "The national solar radiation data base (NSRDB)," *Renew. Sustain. Energy Rev.*, vol. 89, pp. 51–60, Jun. 2018, doi: 10.1016/j.rser.2018.03.003.
[34] C. A. Gueymard, "Direct and indirect uncertainties in the prediction of tilted irradiance for solar engineering applications," *Sol. Energy*, vol. 83, no. 3, pp. 432–444, Mar. 2009, doi: 10.1016/j.solener.2008.11.004.
[35] M. Lave, W. Hayes, A. Pohl, and C. W. Hansen, "Evaluation of global horizontal irradiance to plane-of-array irradiance models at locations across the United States," *IEEE J. Photovolt.*, vol. 5, no. 2, pp. 597–606, 2015, doi: 10.1109/JPHOTOV.2015.2392938.
[36] D. R. Myers, T. L. Stoffel, I. Reda, S. M. Wilcox, and A. M. Andreas, "Recent progress in reducing the uncertainty in and improving pyranometer calibrations," *J. Sol. Energy Eng.*, vol. 124, no. 1, pp. 44–50, Feb. 2002, doi: 10.1115/1.1434262.
[37] M. G. Kratzenberg, H. G. Beyer, S. Colle, and A. Albertazzi, "Uncertainty calculations in pyranometer measurements and application," in *Solar Energy*. Denver, CL, USA: ASMEDC, Jan. 2006, pp. 689–698, doi: 10.1115/ISEC2006-99168.
[38] C. Monokroussos et al., "Rear-side spectral irradiance at 1 sun and application to bifacial module power rating," *Prog. Photovolt., Res. Appl.*, vol. 28, no. 8, pp. 755–766, Aug. 2020.